Solar neutrino constraints on U(1)′ models via coherent elastic neutrino-nucleus scattering

M. Demirci*, M. F. Mustamin

Department of Physics, Karadeniz Technical University, Trabzon, TR61080, Türkiye

Abstract

We examine new physics from $U(1)'$ gauge symmetry via coherent elastic neutrino-nucleus scattering (CEνNS) utilizing solar neutrinos. Particularly, we focus on an additional vector boson with an associated $U(1)_{B-L}$, $U(1)_{B-3L_e}$, $U(1)_{B-3L_\mu}$, and $U(1)_{B-3L_\tau}$ gauge symmetries. These models have different fermion charges, which determines their contributions to the CEνNS process. We show effect of these models by incorporating them in signal of the SM using solar neutrino flux. We place new constraints on these models using the recent CDEX-10 data. Our findings indicate that there are some improvements from previous limits.

Keywords: CEνNS, solar neutrino, beyond the SM, B-L models
DOI: 10.31526/ACP.BSM-2023.10

1. INTRODUCTION

The phenomenology of coherent elastic neutrino-nucleus scattering (CEνNS) occurs when neutrinos scatter off a nucleus as a whole [1]. It is difficult to observe experimentally this process because the nuclear recoil energy reaches to low keV region. This is the required criteria to ensure that neutrinos interact as a whole with the nucleus. This phenomenon has first been observed by the COHERENT experiment with neutrinos from pion decay at rest (π-DAR) sources [2, 3]. Since then, it has been triggering scientific works related to this process both theoretically and experimentally. It gives a novel framework to study fundamental parameters of the Standard Model (SM) and physics beyond the SM (BSM).

Utilizing solar neutrinos as a source of inducing the CEνNS process would be an interesting framework, especially for studying BSM physics. One of the densest natural sources of neutrino on the earth is solar neutrinos. The Sun produces electron neutrinos through the nuclear fusion process in its core. The energy of the solar neutrinos that reach the Earth is located in the range of a few MeV scale, relevant to study their interaction with matter. Since its first observation [4], it has been one of the widely worked subjects. The compact study of it is incorporated within the Standard Solar Model [5, 6, 7].

Even though the SM provides a very successful description of EW and strong interactions, it has some frailties that point to an extension of the current theory. Many SM extensions contain low-mass particles from hidden sectors, e.g., grand unified theories, models that explain baryogenesis, or dark sector models. In this work, we study an extension to the SM by incorporating $U(1)'$ symmetry with light neutral vector Z' boson [8]. We particularly examine a few models with $U(1)_{B-L}$ [9, 10] and $U(1)_{B-3L_\ell}$ [11, 12, 13] gauge symmetries. The symbols B, L represent lepton numbers for baryons and leptons, respectively. The index $\ell = e, \mu, \tau$ represents the lepton families of the neutrino flavors.

The additional vector mediator Z' has an interaction term with the quarks and leptons of SM. The couplings from each model differ according to their corresponding $U(1)'$ charges. The scattering experiments could be used to investigate the vector mediator Z' by measuring the deviation of the scattering cross section from its SM prediction. All of them are well motivated as theoretical to provide additional explanations to a series of precision studies in low-energy observables of CEνNS with solar neutrinos.

We provide constraints on the coupling-mass parameters of additional vector mediator Z' via CEνNS using the CDEX-10 data [14, 15]. The CDEX experiment [16] has the main goal of observing light DM. It has recently detected neutrino-nucleus signals from solar neutrino flux using a germanium target. In the data, event rates are given according to the electron equivalent recoil energies. These values are converted to nuclear recoil signals with the help of a quenching factor. Furthermore, our results are compared with the available constraints of previous works.

The structure of the remainder of this work is as follows. In Sec. 2, we review analytical expressions of the CEνNS in the SM and $U(1)'$ models. In Sec. 3, we present the analysis method used for limit setting. In Sec. 4, we present the expected event spectra of both the SM and the considered $U(1)'$ models. We show the upper-limits of the parameter space and compare these with previously available limits. Finally, in Sec. 5, we summarize our work.

2. THEORETICAL FORMULATION

2.1. CEνNS Cross-section

In the CEνNS process, a neutrino with initial energy E_ν scatters from a nucleus target and transmits a kinetic recoil energy T_{nr} to the nucleus. The process happens as the neutrino interacts with the nucleus as a whole. For the transfer momentum $|\vec{q}| \lesssim \frac{1}{R}$ with the typical nuclear size R, the coherent scattering can provide a cross section enhancement.

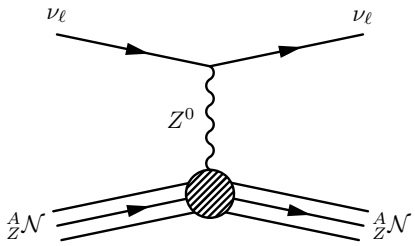

FIGURE 1: Feynman diagram for CEνNS in the SM. Details are in the text.

In Fig. 1, the representative diagram of CEνNS for the SM is shown. We use $^A_Z\mathcal{N}$ tp represent a nucleus with A nucleons and Z protons. The Z^0 represents the SM neutral vector boson. The subscript ℓ stands for $\ell = e, \mu$ or τ. The differential cross-section of this process in the SM is given by

$$\left[\frac{d\sigma}{dT_{nr}}\right]_{\rm SM} = \frac{G_F^2 m_{\mathcal{N}}}{\pi} Q^2_{\rm SM}\left(1 - \frac{m_{\mathcal{N}} T_{nr}}{2E_\nu^2}\right)\left|F(|\vec{q}|^2)\right|^2, \tag{1}$$

where G_F is the Fermi constant, m_N is the nucleus mass, and T_{nr} is the nuclear recoil energy. The weak nuclear charge $Q_{\rm SM}$ is written as

$$Q_{\rm SM} = g_V^p Z + g_V^n N. \tag{2}$$

The proton and neutron couplings in this relation are given by

$$g_V^p = 1/2(1 - 4\sin^2\theta_W), \quad g_V^n = -1/2, \tag{3}$$

respectively. Here, we set the value of $\sin^2\theta_W = 0.23863$ [17] (low momentum transfer in the $\overline{\rm MS}$ scheme). It should be noted that the SM cross section of the process is independent of flavor at the tree level. There are flavor dependencies in the small loop corrections, however they have no significant impact on the current sensitivities [18]. The weak nuclear form factor is given by $F(|\vec{q}|^2)$, which defines the internal structure of the target nucleus. We use the same Helm form factor [19] for the neutron and proton, namely $F = F_n \simeq F_p$.

2.1.1. *Contributions from $U(1)_{B-L}$, $U(1)_{B-3L_e}$, $U(1)_{B-3L_\mu}$, and $U(1)_{B-3L_\tau}$ models*

There are plentiful works regarding SM extensions with additional $U(1)'$ gauge group with an associated neutral vector gauge boson Z' [20]. A requirement for such models is that it has to be anomaly-free. This criterion is created by expanding the SM with three right-handed neutrinos. The addition simultaneously describes the smallness of neutrino mass via see-saw mechanism [21, 22, 23]. Furthermore, these models can clarify several unsolved puzzles in the SM such as the grand unified theory, nature of DM, baryogenesis mechanism through leptogenesis, and also explain anomalies from recent experiments.

In the present work, we investigate an extra vector Z' mediator with an associated $U(1)'$ gauge group for a variety of models. We consider the $U(1)_{B-L}$ [9, 10], $U(1)_{B-3L_e}$, $U(1)_{B-3L_\mu}$, and $U(1)_{B-3L_\tau}$ [11, 12, 13] models. The generic Lagrangian is given by [24, 25]

$$\mathcal{L}_{Z'} = Z'_\mu\left[\sum_{q=u,d} Q'_q g^q_{Z'} \bar{q}\gamma^\mu q + Q'_\ell g^{\nu_\ell}_{Z'} \bar{\nu}_{\ell L}\gamma^\mu \nu_{\ell L}\right] \tag{4}$$

where the vector coupling constant $g^q_{Z'}$ is for quarks and $g^\nu_{Z'}$ for neutrinos. The $U(1)'$ charges of quark and neutrino are denoted by Q'_q and Q'_ℓ. We apply these charges for a generalized form of anomaly free UV-complete models including only the SM particles plus right-handed neutrinos [26]. The Z' mediator contribution to the CEνNS is written as

$$\left[\frac{d\sigma}{dT_{nr}}\right]_{Z'} = \frac{Q^2_{Z'} m_{\mathcal{N}}\left|F(|\vec{q}|^2)\right|^2}{2\pi(m^2_{Z'} + 2m_{\mathcal{N}}T_{nr})^2}\left(1 - \frac{m_{\mathcal{N}}T_{nr}}{2E_\nu^2}\right), \tag{5}$$

where $Q_{Z'}$ represents the weak charge for the nucleus. Conservation of vector current implies that only valence quarks contribute by adding their charges, hence one has

$$Q_{Z'} = \left[Z\sum_q Q'_q g^q_{Z'} + N\sum_q Q'_q g^q_{Z'}\right] Q'_\ell g^{\nu_\ell}_{Z'}. \tag{6}$$

The considered $U(1)_{B-L}$ and $U(1)_{e,\mu,\tau}$ models differ in terms of the fermion charges with the associated gauge group. The charge of quarks for each model is $Q'_{u,d} = 1/3$. For the lepton charges, in the $B-L$ model we have the $Q'_{e,\mu,\tau} = -1$, while for the $B - 3L_\ell$

we have $Q'_{\ell=e,\mu,\tau} = -3$. Because both the SM and the Z' have vector type interactions, they hence contribute coherently to the CEνNS cross section. We notice that the Z' mediator models do interfere with the SM case, so the full cross section reads

$$\left[\frac{d\sigma}{dT_{nr}}\right]_{\mathrm{SM}+Z'} = \left[1 + \frac{Q_{Z'}}{\sqrt{2}G_F Q_{\mathrm{SM}}(m_{Z'}^2 + 2m_{\mathcal{N}}T_{nr})}\right]^2 \left[\frac{d\sigma}{dT_{nr}}\right]_{\mathrm{SM}}. \tag{7}$$

The last three models, namely the $B-3L_{\ell}$,. depend on different neutrino flavors. Because of this, we consider the solar neutrino survival probabilities in these models. For the case of $\nu_e \to \nu_e$, $\nu_e \to \nu_\mu$, and $\nu_e \to \nu_\tau$ the probabilities are

$$P_{ee} = P_{eff}\cos^4\theta_{13} + \sin^4\theta_{13}, \tag{8}$$

$$P_{e\mu} = (1 - P_{ee})\cos^2\theta_{23}, \tag{9}$$

$$P_{e\tau} = (1 - P_{ee})\sin^2\theta_{23}, \tag{10}$$

respectively, while P_{eff} is the factor of the matter effect given as [17]

$$P_{eff} = \sin^2\theta_{12}. \tag{11}$$

We consider this form for solar neutrinos in a few MeV energy. The parameters in these probabilities are set to the best-fit central values of the recent oscillation parameters with normal ordering [27].

2.2. *Differential Rate*

We obtain the event rate by the convolution of cross section with neutrino flux as

$$\frac{dR}{dT_{nr}} = N_T \int_{E_\nu^{min}}^{E_\nu^{max}} dE_\nu \frac{d\Phi(E_\nu)}{dE_\nu}\frac{d\sigma(E_\nu, T_{nr})}{dT_{nr}}, \tag{12}$$

where $d\Phi(E_\nu)/dE_\nu$ is the differential neutrino flux. The factor $N_T = m_t N_A/m_A$ is the number of target nuclei per unit mass of the detector material. The minimum and maximum incoming neutrino energy are denoted by E_ν^{min} and E_ν^{max}, respectively. The minimum neutrino energy satisfies

$$E_\nu^{min} = \frac{T_{nr}}{2}\left(1 + \sqrt{1 + \frac{2m_{\mathcal{N}}}{T_{nr}}}\right), \tag{13}$$

which is required to trigger the nuclear recoil energy. We fix the maximum neutrino energy to the end point of the solar neutrino flux. Meanwhile, the maximum nuclear recoil energy satisfies

$$T_{nr}^{max} = \frac{2E_\nu^2}{2E_\nu + m_{\mathcal{N}}}. \tag{14}$$

Here, it is clear that lighter nuclei enhance the maximum nuclear recoil energy produced in the detector.

We implement solar neutrino flux from the BS05(OP) standard solar model (SSM) [28, 29]. There are eight neutrino fluxes which originate from the proton-proton (pp) chain and Carbon-Nitrogen-Oxygen (CNO) cycle inside the sun. In the pp chain, neutrinos are produced via five nuclear reactions called as the ^{7}B, ^{8}Be, pp, pep, and hep. In the CNO cycle, neutrinos are commonly produced via decays of ^{13}N, ^{15}O, and ^{17}F.

The detector in the experiment observes an electron equivalent energy T_{ee}, which is different from the nuclear recoil energy signal as neutrinos scatter off the nuclei. These two quantities are related using quenching factor $Y(T_{nr})$. We consider the Lindhard quenching factor [30]

$$Y(T_{nr}) = \frac{kg(\epsilon)}{1 + kg(\epsilon)} \tag{15}$$

with

$$g(\epsilon) = 3\epsilon^{0.15} + 0.7\epsilon^{0.6} + \epsilon, \tag{16}$$

$$\epsilon = 11.5Z^{-7/3}T_{nr}, \tag{17}$$

where we set $k = 0.162$ in this work. The value of k is chosen from the latest measurement in the low-energy range [31, 32]. With the quenching factor, the nuclear recoil energy T_{nr}(keV) is converted into electron equivalent T_{ee}(keV) as

$$T_{ee} = Y(T_{nr})T_{nr}. \tag{18}$$

From this relation, the differential rate can be expressed with

$$\frac{dR}{dT_{ee}} = \frac{dR}{dT_{nr}}\frac{1}{Y(T_{nr}) + T_{nr}\frac{dY(T_{nr})}{dT_{nr}}}. \tag{19}$$

3. DATA ANALYSIS METHOD

We analyze the recent CDEX-10 data [15] with associated coherent neutrino-nucleus scattering. The CDEX experiment is part of the China Jinping Underground Laboratory (CJPL) [16]. It has been designed for direct detection of DM, using ultra-low energy threshold pPCGe detectors. Since it first started, some exotic physics searches has been carried out such as axion particles, WIMP, and dark photons. The configuration of the CDEX-10 experimental have been presented in Ref. [14]. The CEνNS, as well as neutrino-electron, process can improve the current limits of the light mediator models in the ROI of DM direct detection endeavors. Accordingly, we consider the recent CDEX-10 data related to neutrino-nucleus scattering.

We use the pull approach of the χ^2 function [34]

$$\chi^2 = \min_{(\xi_j)} \sum_{i=1}^{20} \left(\frac{R^i_{obs} - R^i_{exp} - B - \sum_j \xi_j c^i_j}{\Delta^i} \right)^2 + \sum_j \xi_j^2 \tag{1}$$

where R^i_{obs} and R^i_{exp} are the observed and expected event rates (which consists of SM plus new physics contribution) of the i-th energy bin, respectively. Δ^i denotes experimental uncertainty which includes statistical and systematic uncertainties, for the i-th energy bin. The function is minimized with respect to all pull parameters ξ_j [34]. The c^i_j denotes solar neutrino flux uncertainties. Using this function, we derive the 90% C.L. with two d.o.f. limits of our considered models and further compare them with previous related works that are explained in the next section.

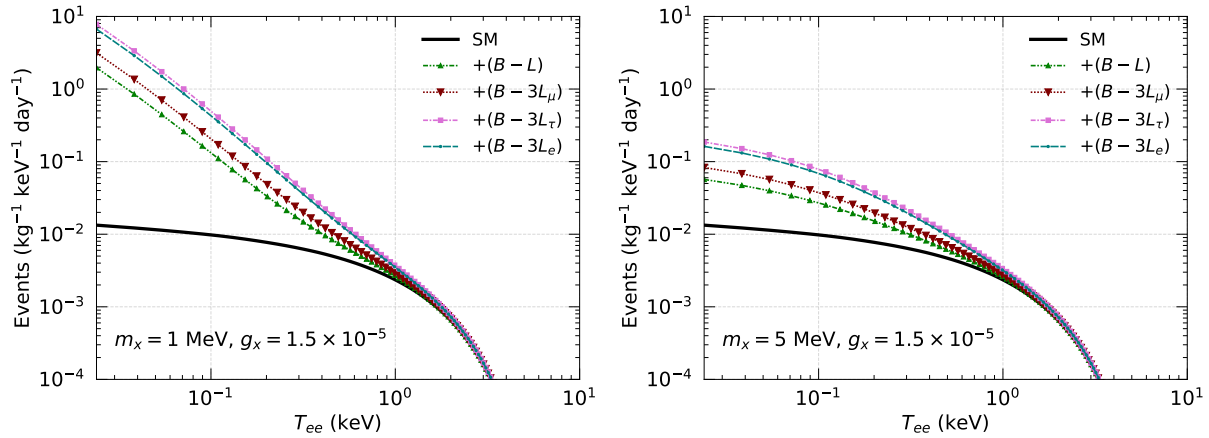

(a) (b)

FIGURE 2: Predicted CEνNS differential rates as a function of nuclear recoil energy for the SM and the U(1)′ models with a mass of 1 MeV (a) and 5 (MeV). Here we implement the ^{8}B neutrino flux which has a large energy spectrum on the Earth.

4. NUMERICAL RESULTS

4.1. Expected Event Spectra

The predicted CEνNS event rates in terms of $T_e e$ for the SM and the U(1)′ models are given in Fig.2. We indicate the coupling constants of the mediators as $g_X = \sqrt{g^q_X g^{\nu_l}_X}$ with the subscript $X = B - L$, $B - 3L_e$, $B - 3L_\mu$, and $B - 3L_\tau$. They are normalized in $\mathrm{kg}^{-1}\,\mathrm{keV}^{-1}\,\mathrm{day}^{-1}$ to match the CDEX-10 data. For representative purposes, we fix the coupling constant as $g_X = 1.5 \times 10^{-5}$ and the mediator mass as 1 MeV in Fig.2.(a) and 5 MeV in Fig.2.(b). Furthermore, the energy resolution of the experiment has also been implemented [15].

From these results, the Z' contribution of the $U(1)'$ models has considerable effects at small recoil energy. These contributions are clearly seen for the mediator with lighter mass. It can be seen that in the high nuclear recoil energy region, their contributions are almost not separated from the SM signal. Notice that the models differ in the fermion charges that determine their contributions to the CEνNS of the interactions mediated by the Z'. We observe this effect from the rates of the $B - L$ model that are relatively smaller compared to the $B - 3L_\ell$ models. These contributions add coherently to the SM weak neutral current interaction. From the chosen benchmarks, it is clear that the lighter mass choice enhances the new physics interaction spectrum while the heavier one suppresses the rates.

4.2. Constaints on the $U(1)'$ models

We show constraints on the coupling-mass parameters with 90% C.L. for the $B - L$ model from CDEX-10 data in Fig.3 while we overlaid this result with previous studies. These bounds are from accelerators, such as LSND [35], CHARMII [36], and the recent report from NA64 [37], as well as nuclear reactors from GEMMA [38]. We also include the limit from COHERENT [2, 3] with

CsI+Ar. We additionally include constraints that explain scalar thermal DM [39]. We also include limits from colliders experiments such as BaBar [40], LHCb[41], KLOE[42], Mainz [43], PHENIX [44], and NA48/2 [45]. Our analysis indicates that CDEX-10 data improved previous bounds in some regions.

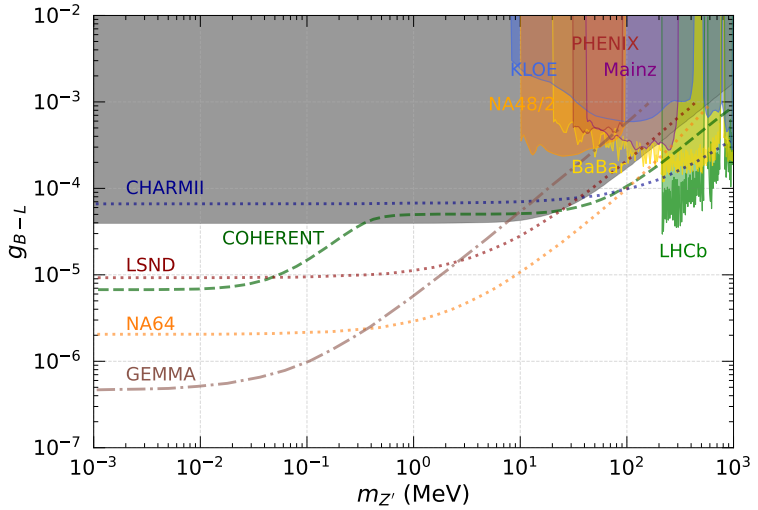

FIGURE 3: 90% C.L. (2 d.o.f.) constraints on the mass-coupling plane of the $U(1)_{B-L}$ model from CEνNS by using current CDEX-10 data and comparison with some constraints from other experiments.

For the B-L model, we reach the upper-limit of $g_{B-L} \lesssim 3.93 \times 10^{-5}$ in the region of $m_{Z'} \lesssim 0.1$ MeV. Our analysis results in more stringent results than the COHERENT limit in the region of 0.34 MeV $\leq m_{Z'} \leq$ 23 MeV. The CHARMII limit is covered as the mediator mass $m_{Z'} \leq 42.4$ MeV, while the GEMMA bound is covered as $m_{Z'} \geq 7.6$ MeV, and slightly better than the LSND result for $m_{Z'} \geq 26$ MeV. The NA64 limit is yet to be reached. Compared to the constraints from colliders, our analysis covers them in the mass range from 8 MeV to 1 GeV.

We show 90% C.L. constraints on the coupling-mass parameters of the $B-3L_e$, $B-3L_\mu$, and $B-3L_\tau$ models in Figs.4 (a), (b), and (c), respectively. Current limits from previous works are also shown in the same figures for comparison. These are derived from π-DAR at COHERENT in Ref. [25], colliders at BaBar [40] and LHCb [41], neutrino scattering with the nucleus at CCFR [46], as well as neutron-lead scattering [47] experiment. We also include results from oscillation derived in Ref. [48] for each model. Particular to the $B-3L_\tau$, we include bound prediction of pion and kaon decays. In general, this result indicates a more stringent limit to some of the mentioned works while yet to reach others.

Our results indicate improvements in some previous limits while yet to fully cover others in the last three models. The $B-3L_e$ result is shown in Fig.4.(a). The upper limit of coupling constant g_{B-3L_e} varies in the range of $3.06 \times 10^{-5} \lesssim g_{B-3L_e} \lesssim 3.31 \times 10^{-5}$ when the mass $m_{Z'}$ goes from 1.0 MeV to 10 MeV. It is seen from the comparison with other limits, that the COHERENT result is fully covered by this work's limit, while the oscillation limit is reached as $m_{Z'} < 2.07$ MeV within the considered parameter space. Moreover, it mainly includes the limit of BaBar. In Fig.4.(b), we show constraints on $B-3L_\mu$ model derived from our analysis, CCFR, COHERENT, LHCb and Oscillation. The coupling constant of g_{B-3L_μ} reaches an upper limit in the range of $3.07 \times 10^{-5} \lesssim g_{B-3L_\mu} \lesssim 3.34 \times 10^{-5}$ for 1.0 MeV $\lesssim m_{Z'} \lesssim$ 10.0 MeV. It covers most of the CCFR limit in the low mass region. However, the COHERENT and oscillation limits are yet to be reached. Furthermore, the LHCb bound is partially covered in the high mass region. Finally for the $B-3L_\tau$, we present the excluded region by our analysis in Fig.4.(c). The obtained limit is in the range of $1.64 \times 10^{-5} \lesssim g_{B-3L_\tau} \lesssim 2.05 \times 10^{-5}$ for 1.0 MeV $\lesssim m_{Z'} \lesssim$ 10.0 MeV. It is clear from comparison with other limits, our result indicates that the current study could explain the kaon and pion decays, as well as the limit from neutron-lead scattering. The oscillation limit is yet to be reached.

In general, our results provide competitive bounds from some existing limits of previous studies. The COHERENT limits are outperformed in the $B-3L_e$ for the considered mass region while in the $B-3L_\mu$ it still dominates for higher mass scale. Also in this model, the CCFR is competitive for massive mediator regions. As for collider results of LHCb and BaBar, both are partially covered and competitive in high mass areas. Moreover, analysis of $B-3L_\tau$ suggests the CDEX-10 data dominating limits from some previous works. Finally, the oscillation limit is all covered in $B-3L_e$ while it outperforms the analysis in both $B-3L_\mu$ and $B-3L_\tau$.

5. SUMMARY AND CONCLUSIONS

In this work, we have investigated new physics from $U(1)'$ models in the process of CEνNS using recent CDEX-10 data. These models are possible for describing novel neutrino-nucleus interactions with light new vector bosons. The differential rate from each model is shown using solar neutrino fluxes, concerning the Linhard quenching factor to convert nuclear recoil energy into its

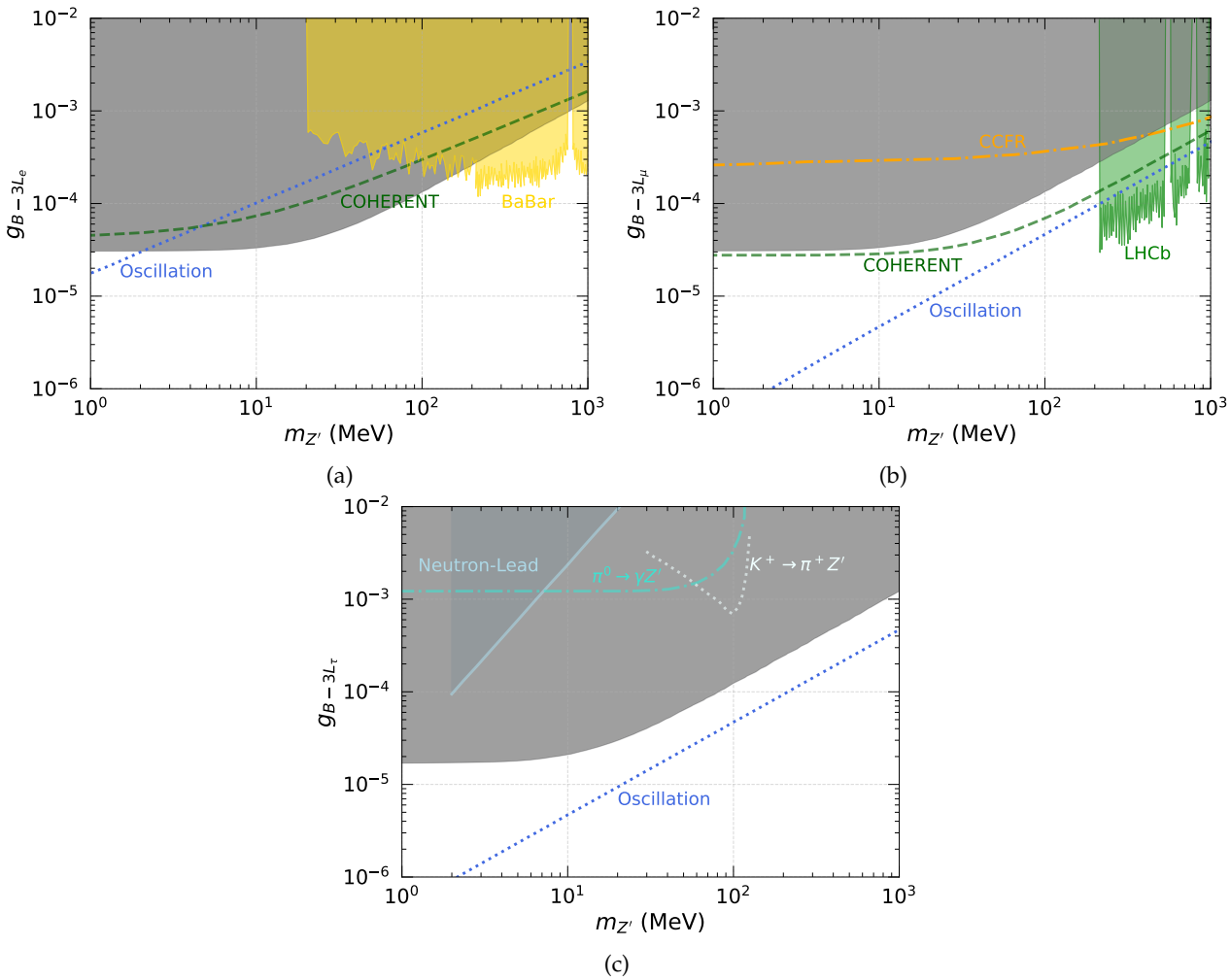

FIGURE 4: 90% C.L. (2 d.o.f.) constraints on the mass-coupling plane of the $U(1)_{B-L}$ (a), $U(1)_{B-3L_e}$ (b), and $U(1)_{B-3L_\mu}$ (c) models from CEνNS by using current CDEX-10 data and comparison with some constraints from other experiments.

electron equivalency. We have placed new bounds on coupling constant - mass plane for the considered $U(1)'$ models using recent data of the CDEX-10 regarding neutrino-nucleus coherent scattering.

We consider a new vector boson that obeys $B-L$, $B-3L_e$, $B-3L_\mu$, and $B-3L_\tau$ gauge symmetries. These considerations could account for possible new physics effects as neutrinos interact with matter, namely quarks components of nuclei. The spectrum of the differential rates for the models has been shown in the case of SM with different types of target nuclei related to relevant experiments. As for the new interactions, we have shown their event rates for the specific target with germanium nuclei, relevant to the considered CDEX-10 data. Several mass scales have been chosen, namely 1 MeV and 5 MeV, with a coupling constant of 1.5×10^{-5} to address new physics behaviour. It is shown that effects of the new interactions have emerged in low-scale nuclear recoil energy, indicating the need for enhancing detector sensitivity in this domain.

Upper-limits at 90% C.L. from two d.o.f. analysis for each model is derived. For the considered $U(1)'$ models, our results indicate some improvements to the current limits while yet to reach others. In the $B-L$ model, some improvements are obtained for CHARM in the low mass, and for LSND and GEMMA in the high mass scales. It also improves the limit from COHERENT in the intermediate mass scale, while it still outperformed in the low and high mass scales. On the other hand, bounds from collider studies are generally covered. However, it does not reach to limit of NA64. In the $B-3L_e$, our analysis dominates over oscillation, and COHERENT, while partially covered BaBar. For the $B-3L_\mu$, we achieve improvements in the low mass region compared to the CCFR and COHERENT limits. However, it is partially covered LHCb and has yet to reach the oscillation limit. Finally, for the $B-3L_e$, it still outperformed by oscillation bound while dominating neutron-lead as well as predicted kaon and pion decay limits.

All in all, we have demonstrated that CEνNS with solar neutrino sources could give some improvements to the available limits. Our results could be utilized to study new physics from U(1)′ models by current and future experimental advancement related to solar and other neutrino sources.

ACKNOWLEDGMENT

This work was supported by the Scientific and Technological Research Council of Türkiye (TÜBİTAK) under the Project no 123F186.

References

[1] D. Z. Freedman, Phys. Rev. D **9**, 1389-1392 (1974).
[2] D. Akimov *et al.* [COHERENT], Science **357**, 1123-1126 (2017).
[3] D. Akimov *et al.* [COHERENT], Phys. Rev. Lett. **126** 012002, (2021).
[4] R. Davis, Jr., D. S. Harmer and K. C. Hoffman, Phys. Rev. Lett. **20**, 1205-1209 (1968).
[5] J. N. Bahcall, M. H. Pinsonneault and S. Basu, Astrophys. J. **555**, 990-1012 (2001).
[6] N. Vinyoles, et al., Astrophys. J. **835**, 202 (2017).
[7] E. Vitagliano, I. Tamborra and G. Raffelt, Rev. Mod. Phys. **92**, 45006 (2020).
[8] M. Demirci and M. F. Mustamin, Phys. Rev. D **109**, 015021 (2024).
[9] R. N. Mohapatra, J. C. Pati, Phys. Rev. D **11**, 566 (1975).
[10] A. Davidson, Phys. Rev. D **20**, 776 (1979).
[11] E. Ma, Phys. Lett. B **433**, 74-81 (1998).
[12] L. N. Chang, et al., Phys. Rev. D **63**, 074013 (2001).
[13] J. Heeck, et al., SciPost Phys. **6**, 038 (2019).
[14] H. Jiang *et al.* [CDEX], Phys. Rev. Lett. **120**, 241301 (2018).
[15] X. P. Geng *et al.* [CDEX], Phys. Rev. D **107**, 112002 (2023).
[16] K. J. Kang *et al.* [CDEX], Front. Phys. (Beijing) **8**, 412-437 (2013).
[17] R. L. Workman *et al.* [Particle Data Group], Prog. Theor. Exp. Phys. **2022**, 083C01 (2022) .
[18] O. Tomalak, P. Machado, V. Pandey and R. Plestid, J. High Energy Phys. **02** (2021) 097.
[19] R. H. Helm, Phys. Rev. **104**, 1466-1475 (1956).
[20] P. Langacker, Rev. Mod. Phys. **81**, 1199 (2009).
[21] R. Harnik, J. Kopp and P. A. N. Machado, JCAP **07**, 026 (2012).
[22] S. Okada, Adv. High Energy Phys. **2018**, 5340935 (2018).
[23] J. Billard, J. Johnston and B. J. Kavanagh, JCAP**11**, 016 (2018).
[24] D. G. Cerdeño, et al., J. High Energy Phys. **05** (2016) 118 [erratum: J. High Energy Phys. **09** (2016) 048].
[25] M. Atzori Corona, et al., J. High Energy Phys. **05** (2022) 109.
[26] B. C. Allanach, J. Davighi and S. Melville, J. High Energy Phys. **02** (2019) 082 [erratum: J. High Energy Phys. **08** (2019) 064].
[27] P. F. de Salas, et al., J. High Energy Phys. **02** (2021) 071.
[28] J. N. Bahcall and A. M. Serenelli, Astrophys. J **626**, 530 (2005).
[29] J. N. Bahcall, A. M. Serenelli and S. Basu, Astrophys. J. Lett. **621**, L85-L88 (2005).
[30] J. Lindhard, V. Nielsen, M. Scharff, and P. V. Thomsen, Kgl. Danske Videnskab., Selskab. Mat. Fys. Medd. 33, 1, (1963).
[31] A. Bonhomme, *et al.*, Eur. Phys. J. C **82**, 815 (2022).
[32] T. Schwemberger and T. T. Yu, Phys. Rev. D **106**, 015002 (2022).
[33] R. Essig, M. Sholapurkar and T. T. Yu, Phys. Rev. D **97**, 095029 (2018).
[34] G. L. Fogli, et al., Phys. Rev. D **66**, 053010 (2002).
[35] L. B. Auerbach *et al.* [LSND], Phys. Rev. D **63**, 112001 (2001).
[36] P. Vilain *et al.* [CHARM-II], Phys. Lett. B **335**, 246-252 (1994).
[37] Y. M. Andreev *et al.* [NA64], Phys. Rev. Lett. **129**, 161801 (2022).
[38] A. G. Beda *et al.* [GEMMA], Phys. Part. Nucl. Lett. **7**, 406-409 (2010).
[39] A. Berlin, et al., Phys. Rev. D **99**, 075001 (2019).
[40] J. P. Lees *et al.* [BaBar], Phys. Rev. Lett. **113**, 201801 (2014).
[41] R. Aaij *et al.* [LHCb], Phys. Rev. Lett. **124**, 041801 (2020).
[42] B. Abelev *et al.* [ALICE], Phys. Lett. B **720**, 52-62 (2013).
[43] H. Merkel *et al.* [A1], Phys. Rev. Lett. **106**, 251802 (2011).
[44] A. Adare *et al.* [PHENIX], Phys. Rev. C **91**, 031901 (2015).
[45] J. R. Batley *et al.* [NA48/2], Phys. Lett. B **746**, 178-185 (2015).
[46] S. R. Mishra *et al.* [CCFR], Phys. Rev. Lett. **66**, 3117-3120 (1991).
[47] R. Barbieri and T. E. O. Ericson, Phys. Lett. B **57**, 270-272 (1975).
[48] P. Coloma, M. C. Gonzalez-Garcia and M. Maltoni, J. High Energy Phys. **01** (2021) 114 [erratum: J. High Energy Phys. **11** (2022) 115].